

BMB Reports – Manuscript Submission

Manuscript Draft

DOI: [10.5483/BMBRep.2022-0149](https://doi.org/10.5483/BMBRep.2022-0149)

Manuscript Number: BMB-22-149

Title: Elevated expression of exogenous RAD51 enhances the CRISPR/Cas9-mediated genome editing efficiency

Article Type: Article

Keywords: CRISPR-Cas9; Double-strand break; Genome editing; Homologous recombination; RAD51

Corresponding Author: Keun Pil Kim

Authors: Seo Jung Park¹, Seo-Bin Yoon¹, Eui-Hwan Choi¹, Hana Hyeon¹, Kangseok Lee¹, Keun Pil Kim^{1,*}

Institution: ¹Life Science, Chung-Ang University,

BMB Reports

Elevated expression of exogenous RAD51 enhances the CRISPR/Cas9-mediated genome editing efficiency

Seo Jung Park¹, Seo-Bin Yoon¹, Eui-Hwan Choi¹, Hana Hyeon¹, Kangseok Lee¹, & Keun Pil Kim^{1,*}

¹Department of Life Science, Chung-Ang University, Seoul 06974, South Korea

*To whom correspondence should be addressed.

Tel.: 82-2-820-5792

Fax: 82-2-820-5206

E-mail: kpkim@cau.ac.kr

Running title: RAD51 enhances CRISPR/Cas9 activity

ABSTRACT

Genome editing using CRISPR-associated technology is widely used to modify the genomes rapidly and efficiently on specific DNA double-strand breaks (DSBs) induced by Cas9 endonuclease. However, despite swift advance in Cas9 engineering, structural basis of Cas9-recognition and cleavage complex remains unclear. Proper assembly of this complex correlates to effective Cas9 activity, leading to high efficacy of genome editing events. To overcome these limitations, we develop a CRISPR/Cas9-RAD51 plasmid constitutively expressing RAD51, which can bind to single-stranded DNA for DSB repair. We show that the efficiency of CRISPR-mediated genome editing can be significantly improved by expressing RAD51, responsible for DSB repair via homologous recombination (HR), in both gene knock-out and knock-in processes. In cells with CRISPR/Cas9-RAD51 plasmid, expression of the target genes (cohesin *SMC3* and *GAPDH*) was reduced by more than 1.9-fold compared to the CRISPR/Cas9 plasmid for knock-out of genes. Furthermore, CRISPR/Cas9-RAD51 enhanced the knock-in efficiency of DsRed donor DNA. Thus, the CRISPR/Cas9-RAD51 system is useful for applications requiring precise and efficient genome edits not accessible to HR-deficient cell genome editing and for developing CRISPR/Cas9-mediated knockout technology.

Keywords: CRISPR-Cas9, DSB, genome editing, RAD51, Homologous recombination

INTRODUCTION

The clustered regularly interspaced short palindromic repeats (CRISPR)/CRISPR-associated protein (Cas)9 has been widely used as a tool for genome engineering (1). This system originated from research on bacterial and archaeal adaptive immune responses in which short sequences from viruses and other mobile genetic elements are incorporated into CRISPR loci in the genome of the host to be transcribed and processed into small RNAs that guide the destruction of invading nucleic acids (2). RNA-programmed DNA editing commences with creating an RNA–DNA hybrid structure between guide RNA (gRNA) and the genomic target sequence using base pair complementarity and a protospacer adjacent motif (PAM) existing next to the target genomic DNA (gDNA) sequence as the engine (3).

An R-loop is a three-stranded nucleic acid structure that comprises RNA–DNA hybrids and single-stranded DNA (ssDNA) displaced from the original DNA duplex (4). This structure functions importantly in many physiological pathways, including regulating gene expression and mediating transcription (5). Nevertheless, R-loops can act as a source of DNA damage, exposing ssDNA that has resulted from RNA–DNA hybridization (6). ssDNA can be a substrate for DNA-damaging agents, and itself is labile (7). Although R-loops have generally been considered to generate only co-transcriptionally, previous findings challenged and suggested that in addition to forming in *cis* at the site of RNA synthesis, R-loops can be formed at sites away from the site of transcription in *trans*. Such *trans*-R-loops are correlated with the CRISPR/Cas9 system (8, 9).

CRISPR/Cas9-mediated genome engineering is conducted at DNA double-strand breaks (DSB) generated at the target gene locus by the HNH and RuvC domains of Cas9 (6-9). The site-specific DSB created by CRISPR/Cas9 then stimulates two main cellular DNA repair mechanisms: non-homologous end joining (NHEJ) and homology-directed recombination (HDR) (10-12). Homologous recombination (HR), the most common form of HDR, accurately restores DSBs using sister chromatids or homologous chromosomes as a homologous template (10-12). RAD51, the key factor of HR machinery as a strand exchange protein that binds to resected ssDNA and forms nucleoprotein filaments, promotes these nucleoprotein filaments to interact with duplex DNA, or its complementary sequence, and generates the synaptic complex for homology search (10-13). Furthermore, RecA, the bacterial strand exchange

protein, has been shown to enhance RNA–DNA hybrid formation *in vitro* (14). A previous study suggested that eukaryotic Rad51, a RecA homolog, promotes the formation of R-loops and influences genomic integrity via a *trans* mechanism in *Saccharomyces cerevisiae* (15). RNA–DNA hybrid forming activity was also suppressed by Srs2, an anti-recombinogenic DNA helicase that functions by unloading Rad51 from ssDNA (16).

A few issues of the CRISPR/Cas9 system come from the mechanism itself. Except the high off-target events, biochemical properties of CRISPR/Cas9 engineering machinery can influence the editing efficiency due to unknown structural basis. The architectural mechanism by which Cas9-sgRNA binary complex detects and breaks target DNA strands is beginning to be elucidated (17-19), highlighting the way to enhance Cas9 function by optimal recruitment and interaction of CRISPR/Cas9 engineering machinery. The inevitable formation of R-loops by the CRISPR/Cas9 system can affect genome editing efficiency as aforementioned. (20, 21). In addition, the stability of DNA-RNA complex influences Cas9 cleavage efficiency based on statistical mechanism analysis (22). Previous work also has shown that the diversity of the single-guide RNA (sgRNA) composition affects the off- and on-target efficiency (21). Thus, elevating the efficiency of targeting for clear editing in the aspect of Cas9-sgRNA-target DNA ternary complex remains an unsolved problem. Here, we demonstrated that expression of exogenous RAD51 promoted not only CRISPR/Cas9-mediated gene knock-in but knock-out, and we established a RAD51-expressing CRISPR/Cas9 system for more effective assembly of RNA-Cas9 ribonucleoprotein (RNP) on target DNA sequences. This suggests the possibility of RAD51 to be utilized as dual key factor in CRISPR/Cas9 genome engineering, also supporting gene knockout based on NHEJ.

RESULTS

Construction of a RAD51-expressing CRISPR/Cas9 system practicable the selection

We created an all-in-one CRISPR/Cas9 vector containing RAD51 expression cassette with enhanced green fluorescence protein (EGFP) and puromycin resistance marker using a gene cloning method. Although we initially wanted to clone the RAD51 expression cassette into the CRISPR/Cas9 plasmid

simply, the efficiency of the original CRISPR/Cas9 plasmid transfection was extremely low. Therefore, the T2A-EGFP sequence was inserted into the lentiCRISPR plasmid to set the condition of transfection (Supplementary Fig. S1A). This selectable marker following the Cas9-FLAG sequence enabled us to confirm the transfection level of the CRISPR/Cas9 plasmid and the expression of Cas9 by fluorescence microscopy. To simultaneously utilize the puromycin resistance marker, the *Bam*HI restriction enzyme sites were used between the FLAG and P2A sequences. To create a CRISPR/Cas9-RAD51-GFP genome editing plasmid, a PCR-amplified linear DNA including E2A-RAD51 followed by a T2A-EGFP sequence was inserted into lentiCRISPR plasmid digested with *Bam*HI restriction enzyme (Supplementary Fig. S1B). Each protein expression of these tri- and quad-cistronic 2A construct was validated using western blotting (Supplementary Fig. S1C).

The generation of cell lines that implement the CRISPR/Cas9 system stably is dependent upon an efficient delivery of the CRISPR/Cas9 system. The CRISPR/Cas9 delivery strategy was optimized using lentiCRISPR-RAD51-GFP plasmid (Supplementary Fig. S1) by checking the GFP expression ratio under various transfection conditions (Fig. 1A, 1B). For the onset of genome editing in the form of plasmid DNA, the transcription and translation of Cas9 are required for a certain period of time (23). After CRISPR/Cas9 vectors were transferred into HEK293T cells, incubation proceeded for 48 h, and the media containing transfection agents was replaced with fresh media 48 h post-transfection. Subsequently, puromycin was added for screening cells transfected with CRISPR/Cas9 plasmid for 72 h.

CRISPR/Cas9-mediated gene knock-out is enhanced by exogenous expression of RAD51

To observe the effect of RAD51 on the working efficiency of CRISPR/Cas9, we targeted the gene encoding glyceraldehyde-3-phosphate dehydrogenase (GAPDH), which is known to be constitutively expressed throughout the cell cycle (24). The product of this gene catalyzes the conversion of glyceraldehyde-3-phosphate to bi-phosphoglycerate in the presence of inorganic phosphate and nicotinamide adenine dinucleotide (24). The CRISPR/Cas9 vectors targeting the *GAPDH* gene were transfected into HEK293T cells and selected with puromycin for 72 h (Fig. 1A, 1B). T7 endonuclease

I (T7E1) detects and cleaves heteroduplexes between strands of nucleic acids mismatched at one or more nucleotides (25). Using this enzyme to evaluate the site-specificity of Cas9, the gDNA surrounding the target locus of the *GAPDH* gene was amplified. Subsequently, the PCR products were denatured and reannealed by heating and gradual cooling. T7E1 was treated to the heteroduplex generated as the output of NHEJ after using the CRISPR/Cas9 system, enabling this heteroduplex to be recognized and cleaved (Fig. 1C). Gel analysis showed a reduction in the parental band intensity relative to that of the negative control, and the enhanced band intensity of the digested bands tended to be higher in RAD51-expressing CRISPR/Cas9 plasmid (Fig. 1D). Amplified PCR products were inserted into TA-vector for single colony sequencing to detect a variety of sequence changes and determine the editing efficiency in the absence of a repair template. Aligned sequences of colonies showed the overall gene knock-out and type of indel occurred by CRISPR/Cas9-gGAPDH and CRISPR/Cas9-RAD51-gGAPDH system (Supplementary Fig. S2A). Efficiency of genome editing, gauged through the fraction of GAPDH wild-type sequences to whole colonies sequences, in CRISPR/Cas9-RAD51-gGAPDH system was elevated by more than 2.5-fold compared to CRISPR/Cas9-gGAPDH system (Supplementary Fig. S2B).

A standard protein analysis was performed to investigate the impact of RAD51 on the CRISPR/Cas9 system at the protein level (Fig. 2A). The result revealed that expression of the target gene was diminished by half in the CRISPR/Cas9-RAD51 plasmid (Fig. 2B). Quantitative PCR (qPCR) for *GAPDH* was performed to confirm the effect of RAD51 at the RNA level (Fig. 2C). Thus, these results suggested that RAD51 promotes the efficiency of CRISPR/Cas9-mediated gene disruption. To apply this genome editing system widely, gene knock-out analysis was additionally performed in NIH3T3 cells. CRISPR/Cas9-RAD51 plasmid, the target sequence of which was transferred into the *GAPDH* sequence of mice, was delivered into NIH3T3 cells. Consistent with the above results, RAD51 highly activated the CRISPR/Cas9 system regarding genomic disruption in the NIH3T3 cell line (Fig. 2D, 2E).

In order to further verify the influence of RAD51 on CRISPR/Cas9 editing, we targeted another gene, one encoding the structural maintenance of chromosomes protein 3 (SMC3). SMC3 is a

subunit of the cohesin complex, which mediates sister chromatid cohesion and facilitates the normal segregation of chromosomes during mitosis or meiosis (11, 26). The rod-shaped cohesion subunits SMC1 and SMC3 dimerize with a globular hinge domain at one end of the 50 nm-long intramolecular antiparallel coiled-coil, interacting with another cohesin subunit (Fig. 3A). The expression level of the *SMC3* gene edited by the CRISPR/Cas9 system was validated using immunoblotting and qPCR analyses. The results showed a two-fold decrease in the protein and RNA levels of *SMC3* (Fig. 3B–D). Besides chromosomal segregation, SMC3 also participates in DNA recombination and repair pathways (26). SMC3 has been identified as the target of the serine/threonine kinase Chk2, which is one of the key checkpoint control factors involved in DNA repair and cell death regulation (27). Considering its relationship with processes affecting genome instability, SMC3 expression level might play a critical role in genomic integrity (26). To identify the phenotypic property of SMC3 knock-out by the CRISPR/Cas9-RAD51 system, we measured cell death using flow cytometry. Then, cell death processes were sorted into three groups: live cells (green), injured cells (blue), and dead cells (pink) (Fig. 3E). The ratio of live cells in exogenous RAD51 expression was slightly increased, implying that expression RAD51 does not affect to cellular damage response. However, the ratio of dead and injured cells was increased more in cells with the CRISPR/Cas9-RAD51 system than in those with the normal CRISPR/Cas9 system (29.51% of cells transfected with CRISPR/Cas9 (gSMC3) plasmid were in the dead cells and 20.13% were in the injured cells; 49.8% of cells transfected with CRISPR/Cas9-RAD51 (gSMC3) plasmid were in the dead cells and 30.12% were in the injured cells.) (Fig. 3F). To certify that effective depletion of SMC3 by CRISPR/Cas9-RAD51 (gSMC3) vector caused the decrease of cell viability, we gauged cell viability in GAPDH-targeting CRISPR/Cas9-system. Supplementary Fig. S3 shows that depletion of GAPDH didn't affect to cell viability. These results indicated that the CRISPR/Cas9-RAD51 system is highly efficient in genome editing, with various applications.

Expression of exogenous RAD51 results in higher knock-in efficiency

Cas9-RAD51-mediated knock-in efficiency was investigated on the overall CRISPR/Cas9 system. The strategy allowing us to observe the efficiency of knock-in optically is shown in Fig. 4A. We designed

the gRNA that can bind directly to terminal sequences of the *GAPDH* gene exon 6. The donor template contains the fluorescent marker gene (DsRed) following the cytomegalovirus (CMV) promoter flanked by about 800 bp homology arms (Fig. 4A). Then, we used it as a donor for HDR in the CRISPR/Cas9 system. The correct insertion of the DsRed cassette into the expected locus was confirmed by amplification of genomic DNA (Supplementary Fig. S4A). Depicted primer set (primer a and b) binds to a genomic locus outside of the homology arms of the target gene. When the knock-in of a fluorescent marker occurs successfully, the amplified products including DsRed cassette have bigger size than normal condition. The resulting PCR products described that the intended sequences were correctly integrated (Supplementary Fig. S4B).

After clarification of the knock-in events, the knock-in efficiency was determined by measurement of the expression level of fluorescent protein (Fig. 4B, 4C). Due to an exogenous promoter in the donor template used, the cells transfected with donor templates can constantly express fluorescent proteins (Fig. 4C). To normalize the DsRed signal intensity emitting continuously without genomic insertion by the CRISPR/Cas9 plasmid, the knock-in efficiency was defined as the increased amount of DsRed signal intensity compared to that of cells transfected with CRISPR/Cas9 plasmid excluding the gRNA sequence and donor template (Fig. 4D). Flow cytometry data revealed that the distribution of the peak of the histogram depends on the DsRed signal intensity and exhibited a higher value in the condition of RAD51 expression (Fig. 4D). Equally, the average value of DsRed intensity nearly doubled under CRISPR/Cas9-RAD51 plasmid than under CRISPR/Cas9 plasmid excluding the gRNA sequence (Fig. 4E). All analysis above using flow cytometry was conducted about GFP(+)/DsRed(+) population gated in Supplementary Fig. S5. The system supporting the increased knock-in efficiency by RAD51 has been previously uncovered (28). Thus, these results indicated that RAD51 also enhances gene integration using a knock-in process (Fig. 4F).

DISCUSSION

In this study, we developed a CRISPR/Cas9-RAD51 system with applications for efficient genome editing at loci not accessible to HR-deficient cell genome editing and for developing knock-out CRISPR

technology. This “one-step vector system” that can be used through general transfection methods as well as virus transduction. However, the vector system does not include viral factors such as integrase that cause random insertion of this vector system into the genome in cells. Therefore, random cleavage by gRNA and off-target are not worrying factors. Compared with the original CRISPR/Cas9 plasmid, CRISPR/Cas9-RAD51 accomplished efficient, targeted genomic manipulations in human HEK293T and NIH3T3 cells without donor template. Using two CRISPR/Cas9 expression systems (GAPDH-targeting and SMC3-targeting), we showed that genomic alteration of corresponding target genes was carried out highly under RAD51 expression (Fig. 4F). Consequently, the concentrations of transcripts and the expression levels of target genes were further decreased, enabling the functional effect of the gene product to shift steeply. Along with knock-out, CRISPR/Cas9-RAD51 successfully placed the fluorescent cassette into the intended locus of the gene of interest in the presence of the donor DNA template as reported. In contrast to previous studies that used RAD51 expression as part of the genome editing strategy, we unexpectedly found that RAD51 increased HDR-mediated CRISPR/Cas9 engineering, by extension, had an impact on the knock-down of gene expression caused by NHEJ-mediated CRISPR/Cas9 genome editing (Fig. 4F). We hypothesize that this discovery may be connected to high levels of DSBs by RAD51's dual role of tightly binding to ssDNA and conducting homology searches (working model in Supplementary Fig. S6). One plausible mechanism involves the stabilization of R-loops by RAD51–ssDNA nucleofilament formation. R-loops form unstably with short sequence RNA (20-nt), releasing the nontarget ssDNA in CRISPR/Cas9-mediated genome engineering (29). After the Cas9–gRNA–dsDNA ternary complex has been built, Cas9 interacts with the nontarget DNA strand to stabilize the kinked structure of the nontarget strand. Furthermore, the conformational change in the Cas9 structure achieves the proper re-positioning of the HNH and RuvC nuclease domains of Cas9 near their respective cleavage sites and R-loop stabilization (4-7, 9, 29). For successful applications of the CRISPR/Cas9 system at target loci, the stable establishment of this structure should be essential. After RNA–DNA hybrid formation by the CRISPR/Cas9 system, ssDNA is displaced from the original DNA helix. Under exogenous expression of RAD51, it may create a nucleofilament on the displaced ssDNA of R-loop by the conventional mechanism of RAD51 (Supplementary Fig. S6). It

could contribute to the stabilization of the RNA–DNA hybrid structure, inhibiting Watson–Crick base-pairing in the target duplex DNA and DNA kinking of the nontarget strand. Consequently, RAD51-ssDNA nucleofilaments on R-loop may be able to improve the on-target score by raising the number of DSBs, allowing gRNA to invade and stably bind to the target region. In other words, both NHEJ- and HR-mediated genome editing can be improved by Cas9-gRNA's effective enhancement of DSB formation on RAD51-mediated R-loop stabilization (Supplementary Fig. S6). In addition, when Cas9-induced DSBs form, HDR can occur as an alternative pathway to NHEJ in the presence of sister chromatids. RAD51 coils around the 3' resected ssDNA of the DSB to create nucleoprotein filaments. These resultant structures start homology search and invasion of the target template (12). As RAD51 is critically involved in this step, the RAD51-expressing CRISPR/Cas9 system naturally promotes gene insertion within the donor DNA template. We thus propose here that RAD51 could affect programmable CRISPR/Cas9 editing in two ways: R-loop stabilization and HR-mediated DSB repair (Fig. 4F). Furthermore, it will be interesting to examine whether replication protein A, an ssDNA-binding protein complex, has a similar effect on genomic disruption using the CRISPR/Cas9 system. Thus, the positional relationship between RAD51 and the Cas9–gRNA–dsDNA ternary complex must be explored in the future.

MATERIALS AND METHODS

Materials and methods are available in the supplemental material.

ACKNOWLEDGMENTS

This research was supported by the National Research Foundation of Korea, funded by the Ministry of Science, ICT & Future Planning (2020R1A2C2011887; 2018R1A5A1025077) and the Chung-Ang University Graduate Research Scholarship in 2021.

CONFLICTS OF INTEREST

The authors declare that they have no conflict of interest.

REFERENCES

1. Cong L, Ran FA, Cox D et al (2013) Multiplex genome engineering using CRISPR/Cas systems. *Science* 339, 819–823.
2. Wiedenheft B, Sternberg SH, Doudna JA (2012) RNA-guided genetic silencing systems in bacteria and archaea. *Nature* 482, 331–338.
3. Anders C, Niewoehner O, Duerst A, Jinek M (2014) Structural basis of PAM-dependent target DNA recognition by the Cas9 endonuclease. *Nature* 513, 569–573.
4. Masukata H, Tomizawa J (1990) A mechanism of formation of a persistent hybrid between elongating RNA and template DNA. *Cell* 62, 331–338.
5. Aguilera A, García-Muse T (2012) R loops: from transcription byproducts to threats to genome stability. *Mol Cell* 46, 115–124.
6. San Martín Alonso M, Noordermeer SM (2021) Untangling the crosstalk between BRCA1 and R-loops during DNA repair. *Nucleic Acids Res* 49, 4848–4863.
7. Crossley MP, Bocek M, Cimprich KA (2019) R-loops as cellular regulators and genomic threats. *Mol Cell* 73, 398–411.
8. Gasiunas G, Barrangou R, Horvath P, Siksnys V (2012) Cas9–crRNA ribonucleoprotein complex mediates specific DNA cleavage for adaptive immunity in bacteria. *Proc Natl Acad Sci U S A* 109, E2579–E2586.
9. Wahba L, Gore SK, Koshland D (2013) The homologous recombination machinery modulates the formation of RNA–DNA hybrids and associated chromosome instability. *eLife* 2, e00505.
10. Choi EW, Yoon S, Koh YE, Seo YJ, Kim KP (2020) Maintenance of genome integrity and active homologous recombination in embryonic stem cells. *Exp Mol Med* 52, 1220–1229.
11. Hong S, Joo JH, Yun H, Kim K (2019) The nature of meiotic chromosome dynamics and recombination in budding yeast. *J Microbiol* 57, 221–231.
12. Kim KP, Mirkin EV (2018) So similar yet so different, The two ends of a double strand break. *Mutat Res* 809, 70–80.

13. Choi EH, Yoon S, Hahn Y, Kim KP (2017) Cellular dynamics of Rad51 and Rad54 in response to postreplicative stress and DNA damage in HeLa cells. *Mol Cells* 40, 143–150.
14. Kasahara M, Clikeman JA, Bates DB, Kogoma T (2000) RecA protein-dependent R-loop formation in vitro. *Genes Dev* 14, 360–365.
15. Zaitsev EN, Kowalczykowski SC (2000) A novel pairing process promoted by *Escherichia coli* RecA protein, inverse DNA and RNA strand exchange. *Genes Dev* 14, 740–749.
16. Krejci L, Van Komen S, Li Y et al (2003) DNA helicase Srs2 disrupts the Rad51 presynaptic filament. *Nature* 423, 305–309.
17. Jinek M, Jiang F, Taylor DW, et al (2014) Structures of Cas9 endonucleases reveal RNA-mediated conformational activation. *Science* 343(6176), 1247997.
18. Nishimasu H, Ran FA, Hsu PD, et al (2014) Crystal structure of Cas9 in complex with guide RNA and target DNA. *Cell* 156(5), 935-949.
19. Anders C, Niewoehner O, Duerst A, Jinek M (2014) Structural basis of PAM-dependent target DNA recognition by the Cas9 endonuclease. *Nature* 513(7519), 569-573.
20. Fu Y, Foden JA, Khayter C et al (2013) High-frequency off-target mutagenesis induced by CRISPR-Cas nucleases in human cells. *Nat Biotechnol* 31, 822–826.
21. Graf R, Li X, Chu VT, Rajewsky K (2019) sgRNA sequence motifs blocking efficient CRISPR/Cas9-mediated gene editing. *Cell Rep* 26, 1098–1103.
22. Xu X, Duan D, Chen SJ (2017) CRISPR-Cas9 cleavage efficiency correlates strongly with target-sgRNA folding stability: from physical mechanism to off-target assessment. *Sci Rep* 7(1), 143.
23. Chen F, Alphonse M, Liu Q (2020) Strategies for nonviral nanoparticle-based delivery of CRISPR/Cas9 therapeutics. *Wiley Interdiscip Rev Nanomed Nanobiotechnol* 12, e1609.
24. Meyer-Siegler K, Mauro DJ, Seal G, Wurzer J, deRiel JK, Sirover MA (1991) A human nuclear uracil DNA glycosylase is the 37-kDa subunit of glyceraldehyde-3-phosphate dehydrogenase. *Proc Natl Acad Sci U S A* 88, 8460–8464.
25. Sentmanat MF, Peters ST, Florian CP, Connelly JP, Pruett-Miller SM (2018) A survey of validation strategies for CRISPR-Cas9 editing. *Sci Rep* 8, 888.

26. Choi EW, Yoon S, Koh YE et al (2022) Meiosis-specific cohesin complexes display essential and distinct roles in mitotic embryonic stem cell chromosomes. *Genome Biol* 23, 70.
27. Seo GJ, Kim SE, Lee YM et al (2003) Determination of substrate specificity and putative substrates of Chk2 kinase. *Biochem Biophys Res Commun* 304, 339–343.
28. Kurihara T, Kouyama-Suzuki E, Satoga M et al (2020) DNA repair protein RAD51 enhances the CRISPR/Cas9-mediated knock-in efficiency in brain neurons. *Biochem Biophys Res Commun* 524, 621–628.
29. Jiang F, Taylor DW, Chen JS et al (2016) Structures of a CRISPR-Cas9 R-loop complex primed for DNA cleavage. *Science* 351, 867–871.

FIGURE LEGENDS

Figure 1. Analysis of CRISPR/Cas9-mediated genome editing efficiency for knock-out manner in exogenous expression of RAD51

(A) Diagrams of CRISPR/Cas9-GFP and CRISPR/Cas9-RAD51-GFP vectors. (B) Schematic flow for delivery of CRISPR-Cas9 system to HEK293T cells using (A) modified vectors. (C) Schematic illustration of T7E1 assay to measure the genomic indel percentage. (D) T7E1 analysis comparing the generation of genomic modification at the target locus by the CRISPR/Cas9 system. Indel (%) was calculated as the intensity ratio of the digested band to the parental band.

Figure 2. Analysis of CRISPR/Cas9/Rad51-mediated gene knock-out efficiency in Hek293 and NIH3T3 cells

(A) Analysis of *GAPDH* knock-out efficiency of CRISPR-Cas9 system; expression level of the target gene (*GAPDH*) was determined by immunoblotting analysis. (B) Quantification of *GAPDH* levels. Protein levels of *GAPDH* in (A) were quantified and normalized to α -tubulin (normalized values are depicted in the bar graph). Error bars indicate the mean \pm SD. ($n = 3$). Statistical significance, $*p < 0.05$, $**p < 0.01$, $***p < 0.001$. (C) Confirmation of target gene expression at mRNA level by qPCR. The

bar graph indicates fold-change values of three CRISPR-Cas9 systems compared with the normal condition. Error bars indicate the mean \pm SD ($n = 3$). (D) Immunoblot analysis for RAD51-mediated CRISPR/Cas9 system in NIH-3T3 derived from mouse embryonic fibroblast cells. (E) Quantitative data for (D) indicated the expression level of GAPDH.

Figure 3. Impact of RAD51 on SMC-targeting CRISPR/Cas9 knock-out process

(A) Compositional structure of mitotic cohesin; SMC3 is indicated in bright red. (B) Expression analysis of SMC3 targeted by CRISPR/Cas9. Protein levels were detected through immunoblot assay. (C) Quantification of SMC3 protein levels in (B). Relative SMC3 protein level to α -tubulin was normalized to the sample of non-transfected mock. Error bars indicate the mean \pm SD. ($n = 3$) Statistical significance, $*p < 0.05$, $**p < 0.01$, $***p < 0.001$. (D) qPCR analysis of *SMC3* gene in each CRISPR/Cas9 plasmid. The fold-change value was normalized to the numerical value of the non-transfected mock. Error bars indicate the mean \pm SD. ($n = 3$) (E) Cell viability assay to observe the effect of SMC3 depletion. Each cell sorting (live, injured, and dead cells) was based on the distributions of mock and H₂O₂-treated samples. (F) The proportion of each cell composition in indicated conditions was quantified.

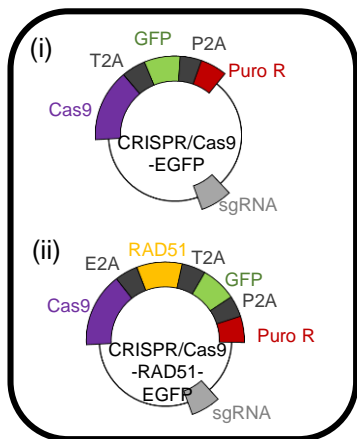
Figure 4. RAD51 promotes the knock-in efficiency of CRISPR/Cas9

(A) Knock-in process of DsRed cassette. sgRNA targeting the terminal region of exon 6 of the *GAPDH* gene cuts that locus, allowing genomic integration of the DsRed cassette through HDR. (B) Cartoon for DsRed-expressing cells by CRISPR/Cas9-mediated knock-in system. (C) Representative images showing DsRed expression in CRISPR/Cas9 system (GFP) through the knock-in process. Due to the exogenous promoter of the DsRed cassette, the expression of DsRed was shown in normal condition. (D) Histogram describes the cell number according to the amount of DsRed intensity in each condition. (E) Quantitative analysis of FL2-H implying DsRed fluorescence measured in (D). Error bars indicate the mean \pm SD. ($n = 3$). Statistical significance, $*p < 0.05$, $**p < 0.01$, $***p < 0.001$. (F) Proposed working mechanism of RAD51-mediated CRISPR/Cas9 system.

Figure 1

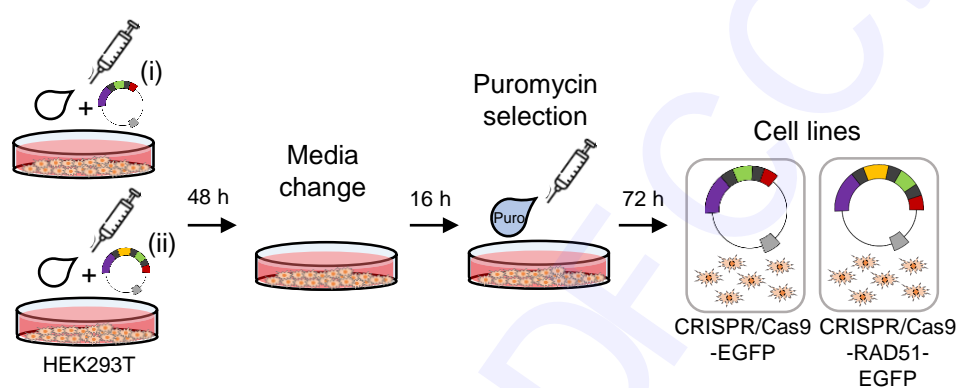
A

Plasmids for transfection



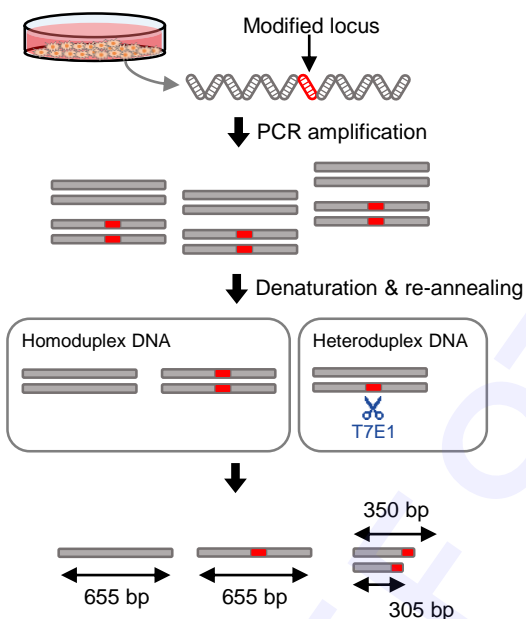
B

Transfection



C

T7 endonuclease I (T7EI) assay



D

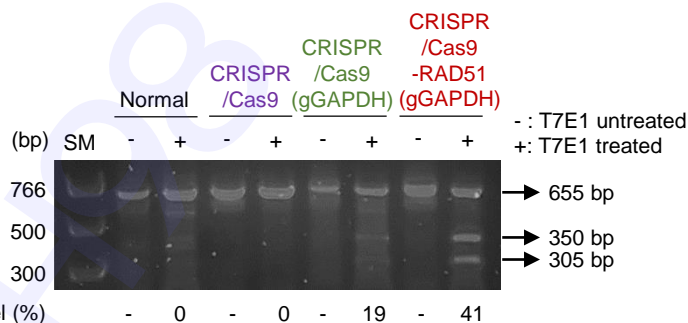
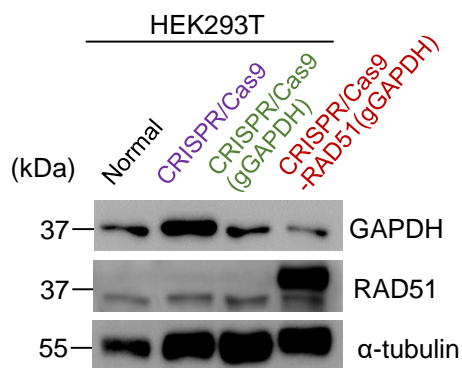
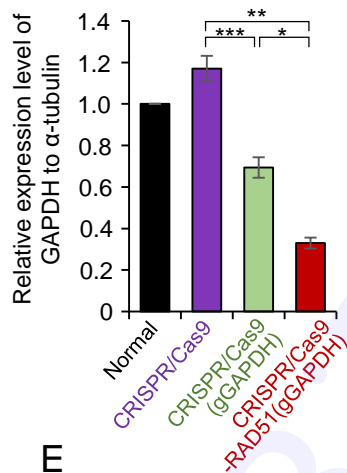


Figure 2

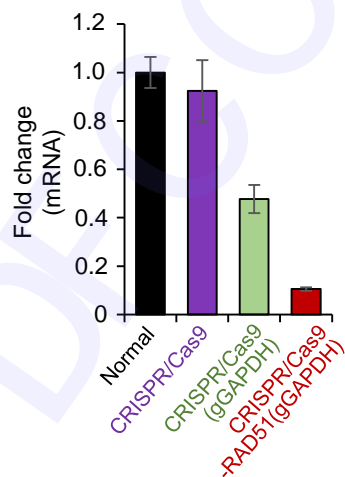
A



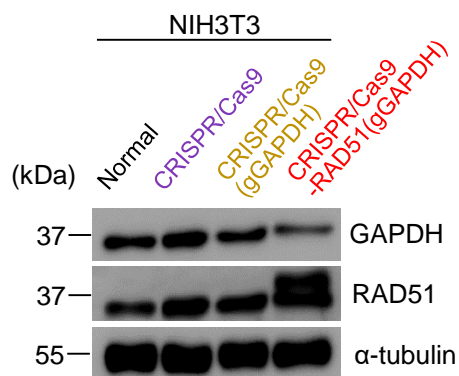
B



C



D



E

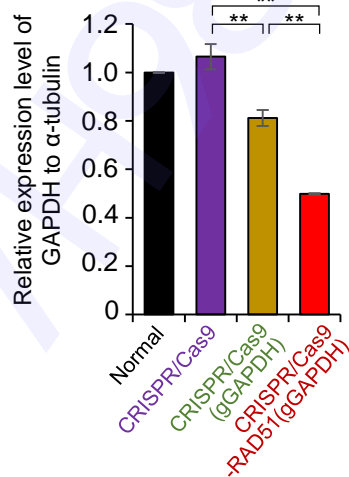


Figure 3

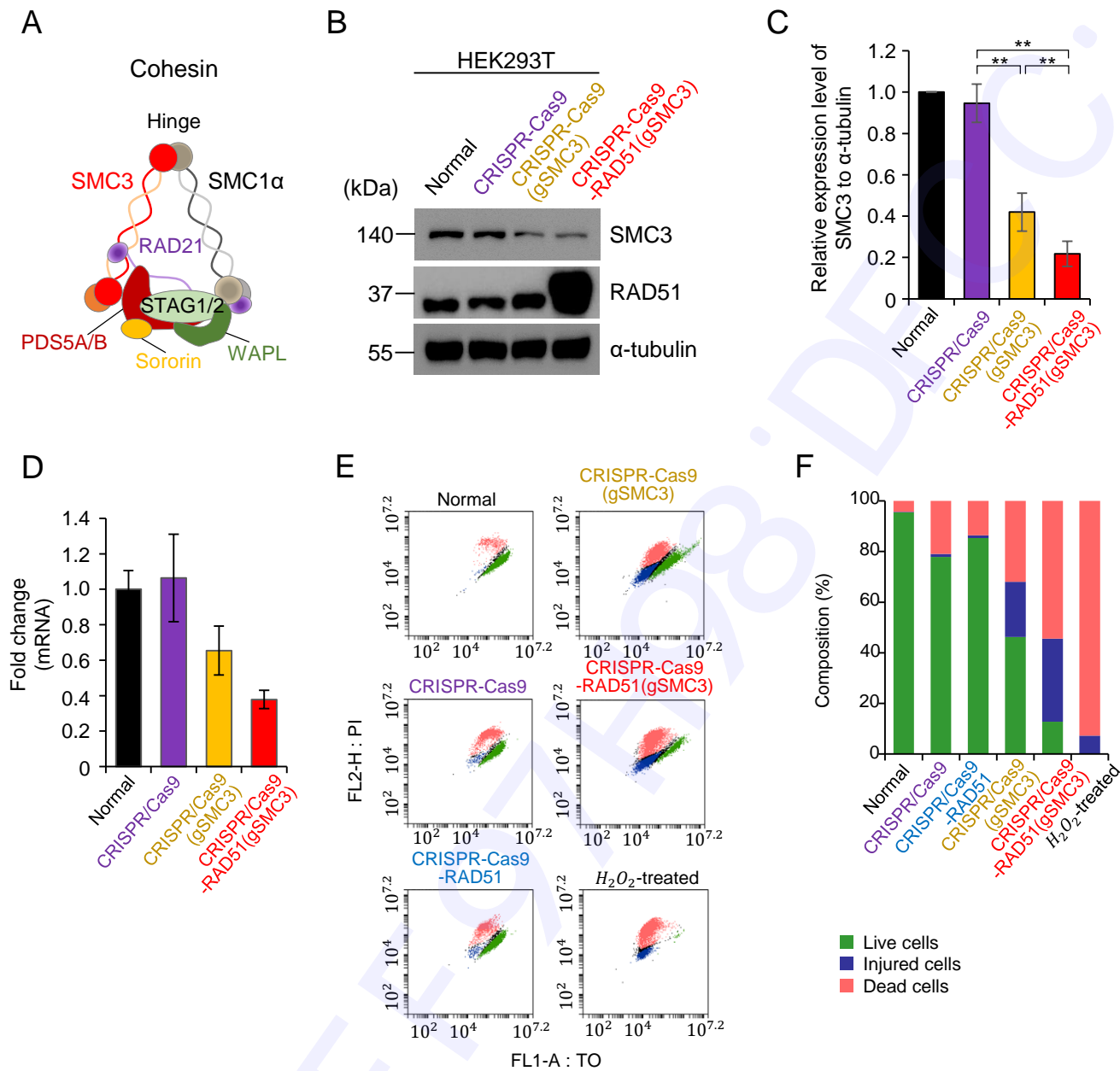
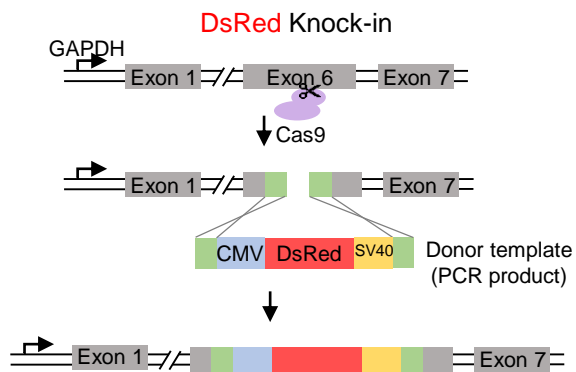
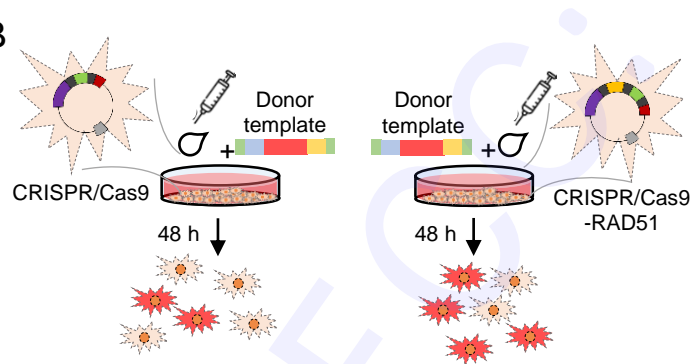


Figure 4

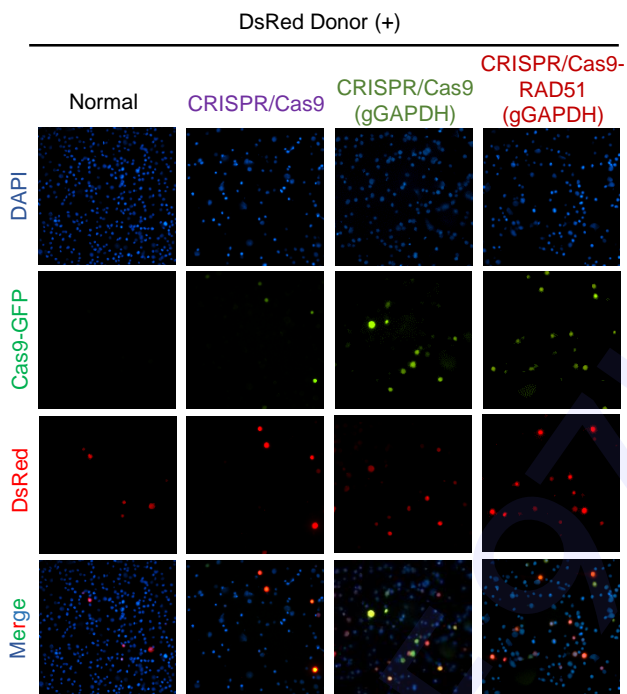
A



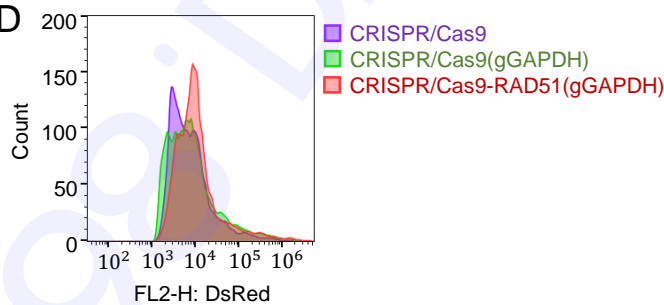
B



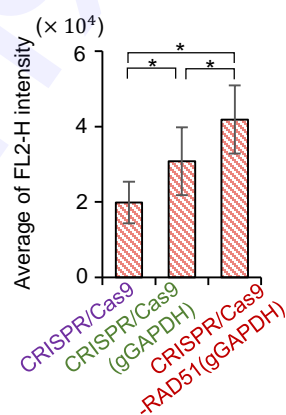
C



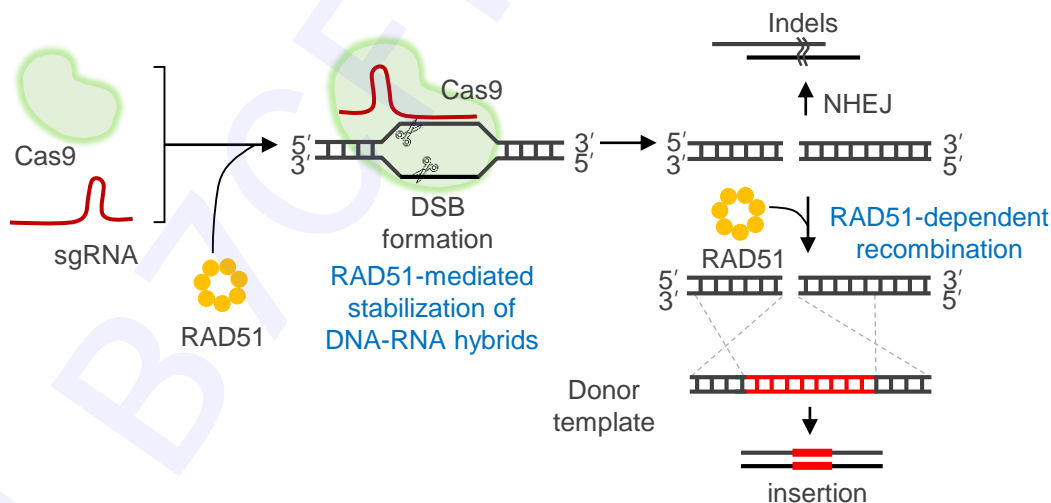
D



E



F



Supplementary Information

**Elevated expression of exogenous RAD51 enhances the
CRISPR/Cas9-mediated genome editing efficiency**

Seo Jung Park¹, Seo-Bin Yoon¹, Eui-Hwan Choi¹, Hana Hyun¹, Kangseok Lee¹, & Keun Pil Kim^{1,*}

¹Department of Life Science, Chung-Ang University, Seoul 06974, South Korea

*To whom correspondence should be addressed.

Tel.: 82-2-820-5792

Fax: 82-2-820-5206

E-mail: kpkim@cau.ac.kr

Running title: RAD51 enhances CRISPR/Cas9 activity

Materials and Methods

Cell culture

HEK293T cells and NIH3T3 cells were grown in Dulbecco's modified Eagle medium supplemented with 10% (v/v) fetal bovine serum and 100 U/ml penicillin/streptomycin. The cells were incubated at 37°C in a 5% CO₂ atmosphere.

Design of the sgRNAs and plasmid constructions

The sequences of each gRNA of the target genes (*GAPDH* and *SMC3*) were designed using the online gRNA design tool developed by the Feng Zhang Laboratory (crispr.mit.edu): *GAPDH* (human): 5'-TTCCTCACCTGATGATCTTG-3'; *GAPDH* (mouse): 5'-ATCCACGACGGACACATTGG-3'; *SMC3* (human): 5'-GAGCTGAGAGAGACAGAAGG-3'. Complementary oligonucleotide pairs were annealed through gradual cooling from 95°C to 25°C, following incubation at 95°C for 5 min. The duplex oligonucleotides include sticky ends with the 5' overhang matched with lentiCRISPR v2 (Addgene plasmid #52961), which was digested with restriction enzyme *BsmB1*. The oligos of sgRNA were ligated into the digested plasmid. Three plasmids were used in the experiments: lentiCRISPR v2-empty-EGFP, lentiCRISPR v2-sgRNA-EGFP, and lentiCRISPR v2-sgRNA-RAD51-EGFP. T2A-EGFP was cloned into lentiCRISPR v2 using *Bam*HI restriction enzyme. Due to the exclusion of a stop codon in the EGFP sequence, it is possible to express the puromycin resistance gene located after the EGFP sequence. To create a plasmid expressing RAD51, which was named lentiCRISPR v2-sgRNA-RAD51-GFP, E2A-RAD51-T2A-EGFP was inserted into lentiCRISPR v2. The genetic construct made for knock-in was originally a plasmid harboring the DsRed cassette (CMV-DsRed-SV40) flanked with homology arms. We amplified a DNA fragment of about 1.6 kb of the *GAPDH* gene sequence containing the target locus in the middle and cloned these fragments into the plasmid backbone. Restriction enzyme sites were introduced near the target locus using inverse PCR, allowing us to insert the DsRed cassette into that site. We obtained the dsDNA template consisting of the DsRed cassette (CMV-DsRed-SV40) flanked by homology arms amplified by PCR.

Transfection and puromycin selection

To perform genetic disruption, 1.2×10^6 HEK293T cells were transfected with 3 μ g of the CRISPR/Cas9 plasmid using 20 μ g polyethylenimine (PEI). In mouse-model, 0.5×10^6 MEFs were transfected with 2.5 μ g of the CRISPR/Cas9 plasmid using lipofectamine 3000 (L3000015, Invitrogen) according to the manufacturer's instruction. Media containing transfection reagents were exchanged with fresh media 48 h post-transfection. For recovery, cells were incubated with fresh media for 12 to 16 h. Puromycin (1 μ g/ml) was applied to the transfected cells for 72 h. For the CRISPR/Cas9 knock-in system, 1.2×10^6 HEK293T cells were co-transfected with 2 μ g of the CRISPR/Cas9 plasmid and 2 μ g of the donor plasmid using 30 μ g PEI. Media containing transfection reagents were replaced with fresh media 48 h post-transfection. For recovery, cells were incubated with fresh media for 12 to 16 h. Puromycin (1 μ g/ml) was applied to the transfected cells for 72 h.

Western blotting

HEK293T cells and MEF cells were resuspended in cell lysis buffer supplemented with a protease inhibitor cocktail containing 1 mM PMSF. Lysate samples were applied on polyacrylamide gels, and after electrophoresis, the proteins in gels were transferred to PVDF membranes. The following antibodies were used, anti-Rad51 (Calbiochem; PC130), anti-FLAG (Santa Cruz Biotechnology; sc-166355), anti- α -tubulin (Abcam; ab4074), anti-GAPDH (Abcam; ab8245), anti-SMC3 (Abcam; ab9263). Immunoreactivity signals were detected using a ChemiDoc™ MP imaging system.

Quantitative PCR

Total RNA was prepared using the RNeasy Mini Kit, according to the manufacturer's instructions. One microgram of total RNA from HEK293T cells was reverse-transcribed using a TOPscript™ reverse transcriptase (Enzymomics). Quantitative (q)PCR was performed using SYBR green and a Bio-Rad real-time PCR system. The concentration of transcript about each gene was normalized with 18s rRNA.

The primer sequences used were as follows, *GAPDH* (human) forward, 5'-TCGGAGTCAACGGATTTGGT-3'; reverse, 5'-TTCCCGTTCTCAGCCTTGAC-3'; *SMC3* (human)

forward, 5'-GATGTGGAGGGCAGTCAGTC-3'; reverse, 5'-GTCCACCTGAAAGCTGTTGC-3', 18s rRNA forward, 5'-GTAACCCGTTGAACCCCAT-3', reverse, 5'-CCATCCAATCGGTAGTAGCG-3'.

Fluorescence-activated cell sorting analysis

To analyze the efficiency of the CRISPR/Cas9 knock-in system, the cells were harvested and washed with Dulbecco's phosphate-buffered saline (DPBS). The cell pellets were fixed overnight with 70% ethanol. The samples were analyzed using an Accuri™ C6 Plus flow cytometer (Becton Dickinson) and quantified with the FlowJo software (Tree Star, Inc).

T7E1 assay

After transfection and puromycin selection, HEK293T cells were then pelleted. gDNA extraction was performed using the Wizard Genomic DNA Purification Kit (Promega) according to the manufacturer's protocol. A region of the *GAPDH* locus containing the target site was amplified using a primer set, forward, 5'-ATCCCTCCAAAATCAAGTGGG-3'; reverse, 5'-TGTGGTCTGCAAAAGGAGTGA-3'. The PCR products were denatured at 95°C for 10 min and then reannealed through ramp down (95°C to 85°C at 2°C/s, then 85°C to 25°C at 0.1°C/s). The consequent heteroduplex was incubated with 5 U of T7E1 (New England Biolabs) at 37°C for 15 min. The digested product was electrophoresed on a 2% agarose gel. Gel analysis was performed using the ImageJ software. The estimated percentage of NHEJ was calculated with the following formula,

$$\%NHEJ \text{ events} = 100 \times [1 - (1 - \text{fraction cleaved})^{(1/2)}]$$

where the fraction cleaved is defined as the density of digested products divided by the density of digested products + undigested parental band.

PCR product cloning and Sanger sequencing

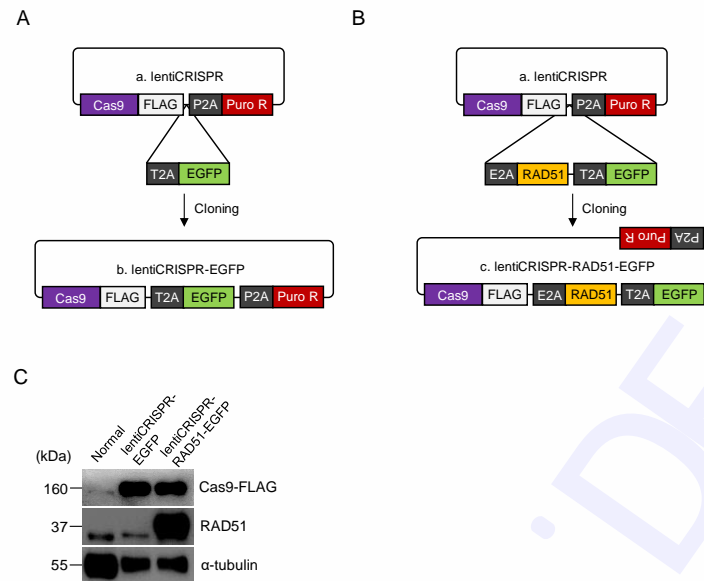
CRISPR/Cas9 targeted regions were validated based on Sanger sequencing (1-3). Purified PCR products from CRISPR/Cas9-treated cells were cloned into vector using All in one™ PCR Cloning Kit (BIOFACT) according to manufacturer's instructions. Sequencing reactions were analyzed on SnapGene.

Cell death assay

To measure cell death, HEK293T cells were suspended in PBS containing thiazole orange and PI. The cells were incubated at 25°C for 5 min. Cell samples were then analyzed on the Accuri™ C6 Plus flow cytometer (Becton Dickinson) and quantified with the Accuri™ C6 software (Becton Dickinson).

Supplementary References

1. Dehairs, J., Talebi, A., Cherifi, Y., & Swinnen, J. V. (2016). CRISP-ID: decoding CRISPR mediated indels by Sanger sequencing. *Scientific reports*, 6, 28973.
2. Jie, H., Li, Z., Wang, P., Zhao, L., Zhang, Q., Yao, X., Song, X., Zhao, Y., & Yao, S. (2017). A simple method based on Sanger sequencing and MS Word wildcard searching to identify Cas9-induced frameshift mutations. *Laboratory investigation; a journal of technical methods and pathology*, 97(12), 1500–1507.
3. Kluesner, M. G., Nedveck, D. A., Lahr, W. S., Garbe, J. R., Abrahante, J. E., Webber, B. R., & Moriarity, B. S. (2018). EditR: A Method to Quantify Base Editing from Sanger Sequencing. *The CRISPR journal*, 1(3), 239–250.

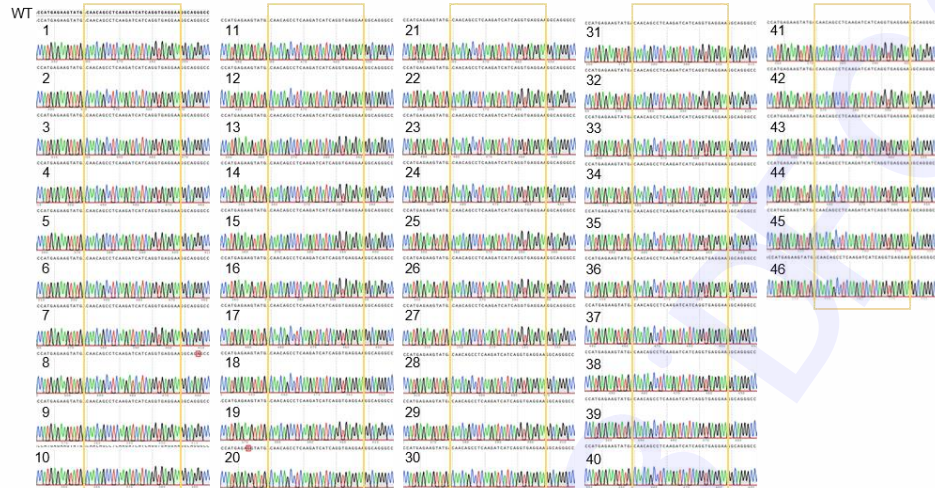


Supplementary Figure S1. Construction of all-in-one CRISPR/Cas9 vector for improvement of genome editing efficiency

(A, B) Experimental schematics of lentiviral CRISPR/Cas9 vector expressing GFP to monitor the efficiency of CRISPR/Cas9 system delivery and expressing RAD51 to promote precise genome modifications. (C) Protein expression analysis using western blotting demonstrated that these 2A constructs are enough to be used as CRISPR/Cas9 system due to constant protein expression level.

A

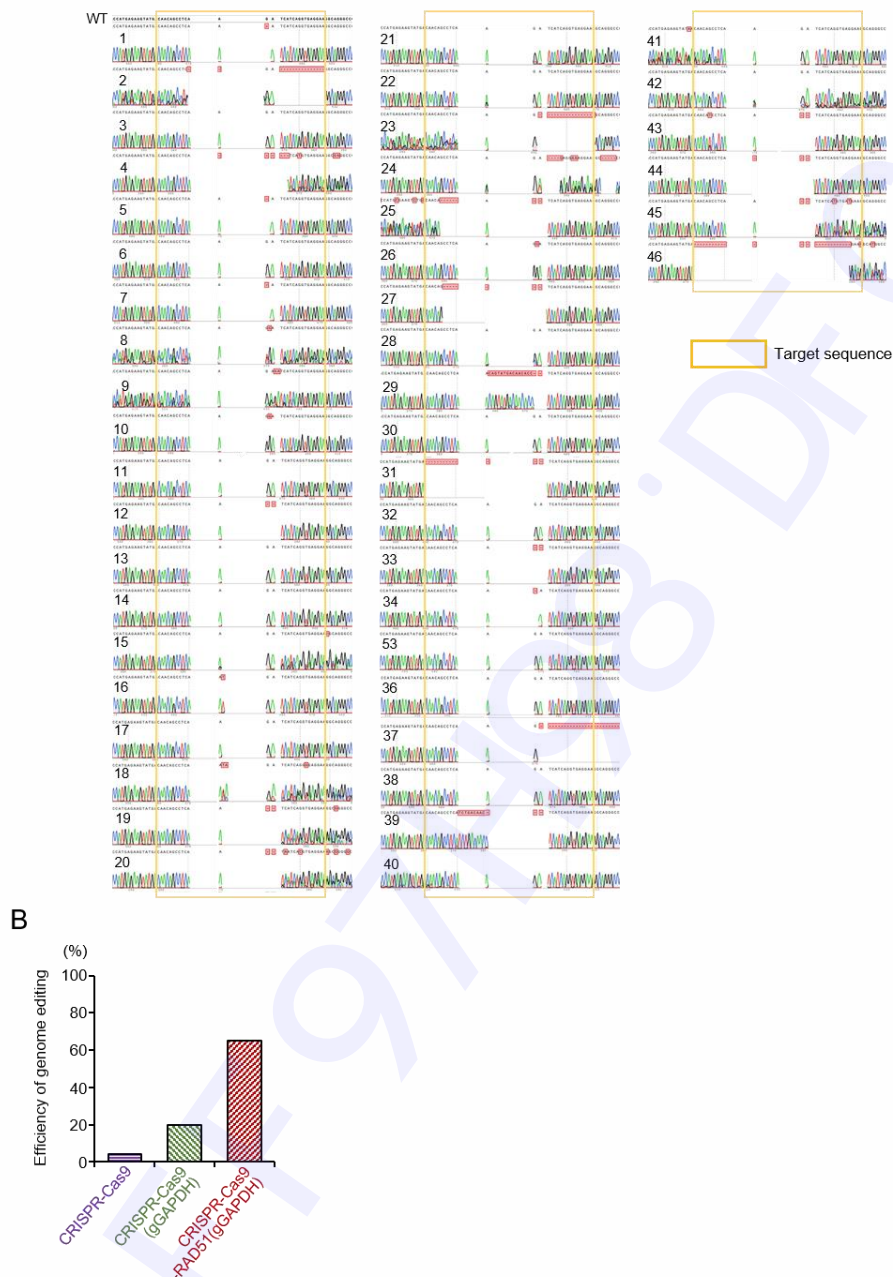
CRISPR-Cas9



CRISPR-Cas9-gGAPDH

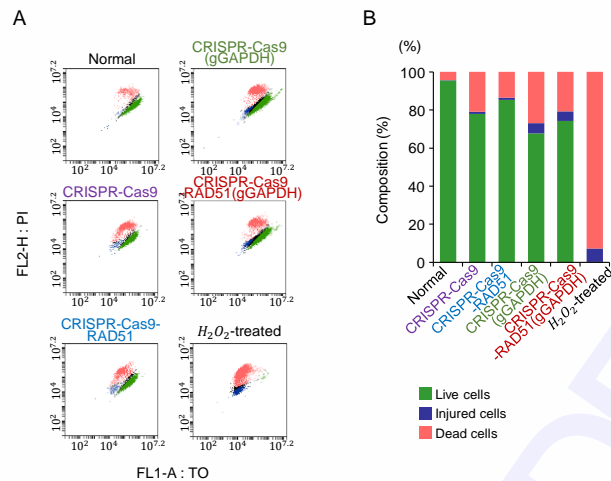
 Target sequence

CRISPR-Cas9-RAD51-gGAPDH



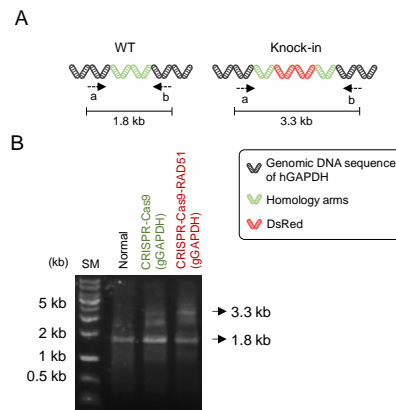
Supplementary Figure S2. Sanger sequencing analysis for GAPDH gene modified by CRISPR/Cas9 system

(A) Sequencing graph of a variety of mutant in CRISPR/Cas9, CRISPR/Cas9-gGAPDH, and CRISPR/Cas9-RAD51-gGAPDH system. Yellow box indicates sgRNA-targeting sequence. Red boxes mark edits including insertion, deletion. (B) The efficiency of genome editing in CRISPR/Cas9, CRISPR/Cas9-gGAPDH, and CRISPR/Cas9-RAD51-gGAPDH system. This value was determined by the ratio of modified sequences to a series of sequences ($n = 46$ for each condition).



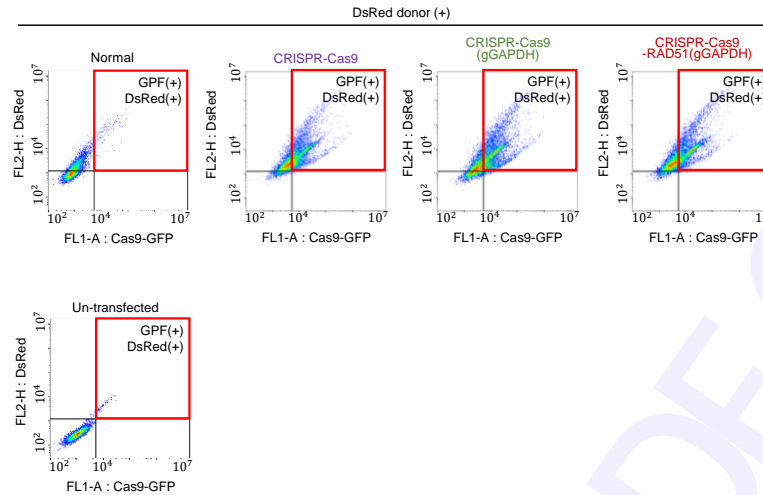
Supplementary Figure S3. Cell viability assay of CRISPR/Cas9-gGAPDH

(A) FACS data showing that depletion of GAPDH doesn't impact to cell viability. each cell sorting (live, injured, and dead cells) was based on the distributions of mock and H_2O_2 -treated samples. (B) The proportion of each cell composition in indicated conditions was quantified.



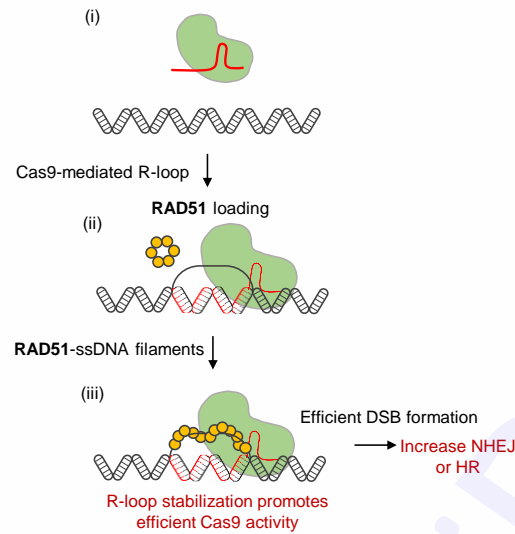
Supplementary Figure S4. PCR analysis for DsRed cassette insertion

(A) Primers designed to check the DsRed cassette insertion into the correct locus. The binding site of each primer is illustrated. (B) PCR fragment analysis using primer (a + b) set. When primer (a + b) set was used, a 1.8 kb fragment indicated the normal condition of the *GAPDH* gene. Fragment of 3.3 kb denotes knock-in of DsRed cassette into *GAPDH* gene.



Supplementary Figure S5. Sorting of cells delivered with CRISPR/Cas9 knock-in system for expression of two fluorescent proteins (GFP, DsRed) using flow cytometry

Scatter plots of cells un-transfected and transfected with only DsRed donor was used as standard of cells classification. The cells were classified as GFP(+) DsRed(+) (top right), GFP(-) DsRed(+) (top left), GFP(-) DsRed(-) (bottom left), and GFP(+) DsRed(-) (bottom right). Considered GFP(+) DsRed(+) cells as successful delivery of CRISPR/Cas9 knock-in system, following statistical analyses were conducted about only this population.



Supplementary Figure S6. A proposed model for RAD51-mediated R-loop stabilization in CRISPR/Cas9 recognition site

Cas9 combined with sgRNA binds to the DNA duplex in a PAM-dependent manner, making the Cas9-sgRNA-DNA complex. sgRNA then invades dsDNA to form an RNA-DNA hybrid with the target DNA strand while displacing the opposite ssDNA. As RAD51 forms nucleofilaments with ssDNA of the displaced nontarget strand, it enables the stabilization of Cas9-mediated R-loops via inhibiting reannealing of dsDNA. The function of RAD51 on the site of the R-loop may promote the activity of Cas9 nuclease, leading to the enhanced efficiency of the CRISPR/Cas9 system.